UC Berkeley
UC Berkeley Previously Published Works

Title

"Measures of Dissipation in Viscoelastic Media" Extended: Toward Continuous Characterization Across Very Broad Geophysical Time Scales

Permalink

https://escholarship.org/uc/item/2g29827z

Journal

Geophysical Research Letters, 46(16)

ISSN

0094-8276

Authors

Lau, Harriet CP
Holtzman, Benjamin K

Publication Date

2019-08-28

DOI

10.1029/2019gl083529

Supplemental Material

https://escholarship.org/uc/item/2g29827z#supplemental

Peer reviewed

Geophysical Research Letters

Key Points:
- Inferences of viscous dissipation across frequencies from earthquakes to convection yield very different estimates of viscosity
- Discrepancies can be explained by spatial variations and/or frequency-dependent mechanical properties
- We propose a framework for inferring transient creep in signals across broad geophysical time scales

"Measures of Dissipation in Viscoelastic Media" Extended: Toward Continuous Characterization Across Very Broad Geophysical Time Scales

Harriet C. P. Lau[1] (ID) **and Benjamin K. Holtzman[2]** (ID)

[1]Department of Earth and Planetary Science, University of California, Berkeley, CA, USA, [2]Lamont Doherty Earth Observatory, Columbia University, Palisades, NY, USA

Abstract We develop a conceptual/quantitative framework whereby measurements of Earth's viscoelasticity may be assessed across the broad range of geophysical processes, spanning seismic wave propagation, postseismic relaxation, glacial isostatic adjustment, and mantle convection. Doing so requires overcoming three challenges: (A) separating spatial variations from intrinsic frequency dependence in mechanical properties; (B) reconciling different conceptual and constitutive viscoelastic models used to interpret observations at different frequencies; and (C) improving understanding of linear and nonlinear transient deformation mechanisms and their extrapolation from laboratory to earth conditions. We focus on (B), first demonstrating how different mechanical models lead to incompatible viscosity estimates from observations. We propose the determination of the "complex viscosity"—a frequency-dependent parameter complementary to other measures of dissipation (including frequency-dependent moduli and attenuation)—from such observations to reveal a single underlying broadband mechanical model. The complex viscosity illuminates transient creep in the vicinity of the Maxwell time, where most ambiguity lies.

1. Introduction

As Earth is subject to forcings with time scales that span milliseconds to billions of years, its rheological response to these processes varies dramatically across the broad spectrum from elastic to viscous behavior. Upon the application of low levels of stress, at depths below the viability of brittle processes, earth materials may exhibit three nonexclusive classes of behavior: (1) purely elastic response, (2) transient creep, and (3) steady state creep. The purely elastic response, in theory, occurs at infinite frequency, and departures from this behavior are a result of mechanical energy dissipation. In oscillatory or self-restoring processes, transient creep can lead to anelasticity, in which deformation is recoverable but dissipative and therefore time dependent. The macroscropic (global-scale) manifestation of dissipation may be observed in the decay of high-frequency body waves propagating through the mantle, the phase lag of Earth tides, and the ongoing lithospheric rebound long after the disappearance of major ice sheets (a phenomenon known as glacial isostatic adjustment, GIA). These processes occur across a wide frequency spectrum, superimposed spatially but with minimal overlap in frequency. Our understanding on the nature of how dissipation is manifest across this spectrum remains incomplete, from geophysical measurement, experiment, and theory.

In their classic study, "Measures of dissipation in viscoelastic media," O'Connell and Budiansky (1978) presented an unambiguous definition of the so-called quality factor, Q, with the intention that a clear presentation of Q might result in a coherently adopted definition across the field of geophysics. Q is a widely used measure of dissipation for which, prior to their study, several possible definitions were applied. Moreover, they highlighted the distinct possibility of mis-estimating intrinsic dissipative properties of a material due to the misinterpretation of the dynamical processes measured at the global scale. We aim to extend the work of O'Connell and Budiansky (1978) here and ask how this consistency can be developed across the entire frequency band of geophysical processes.

Our observational understanding of Earth's dissipation of mechanical energy derives from distinct measurements of geodynamical processes, at different time and length scales. At seismic frequencies (approximately subseconds to minutes), deformation is elastically dominated, while lower-frequency processes involve increasingly more viscous deformation: for example, tidal deformation (approximately hours

to years; Lau et al., 2017; Nimmo & Faul, 2013), postseismic relaxation (approximately hours to years, hereafter "PSR"; e.g., Bürgmann & Dresen, 2008; Freed et al., 2006; Nishimura & Thatcher, 2003; Pollitz et al., 2000), lake rebound (approximately tens to hundreds of years; e.g., Bills et al., 1994; Bills et al., 2007), and GIA (approximately hundreds to millions of years; e.g., Argus et al., 2014; Kaufmann & Lambeck, 2002; Lau et al., 2016; Mitrovica & Forte, 2004; Peltier, 2004). Research on these processes tends to occur in distinct communities across geophysics that adopt preferred viscoelastic models relevant only to the time scale of the processes of interest. The results are seemingly incompatible viscosity estimates of Earth's subsurface (discussed further below) and also contrasting inferences on parameters such as the depth of the lithosphere-asthenosphere boundary (compare western U.S. depth ranges of, for example, 50–80 km inferred from seismic data by Lekic et al., 2011, to 32–65 km inferred using GPS observations of PSR by Dickinson-Lovell et al., 2018, and also the depth of 95 km adopted by Creveling et al., 2017in their GIA study).

Figure 1a shows several estimated viscosities, η, from a variety of studies that have mostly inferred the sublithospheric viscosity around the southwestern region of the United States (with sources listed in the caption). A fundamental conundrum emerges from inferences of viscosity structure from geophysical measurements of surface deformation: *"apparent" viscosity appears to decrease with increasing frequency* (e.g., viscosity inferred from GIA is higher than that from PSR). For every inference of viscosity—be it seismic or geodetic—at least two nonexclusive explanations always exist: (1) spatial variations in *steady state* viscosity reflecting thermodynamic structure; and (2) *transient creep* acting with spatial variations also influenced by thermodynamic structure. For (1), inversion frameworks exist to account for this spatial variation, sampled by any process. For (2), no consistent approach exists to account for the frequency dependence of mechanical response across the broad time scales of processes, which is the focus of this paper. We dissect this conundrum into some combination of three challenges, which will be referred to throughout this paper: (A) separating spatial variations from frequency dependence in mechanical properties; (B) reconciling different conceptual and mechanical models of viscoelasticity used to interpret measurements; and (C) improving our understanding of linear and nonlinear transient deformation mechanisms and how to extrapolate them from laboratory conditions. In section 1.1, we expand upon each of these challenges and in the rest of this paper, we provide a framework for analyzing and seeking consistency in these relationships across the broad frequency spectrum of interest. One might intuitively suppose that these two trends are inconsistent, assuming that if viscosity decreases, attenuation should increase. They can be reconciled when considering that small-strain transient creep mechanisms reduce the apparent viscosity at higher frequency, even though the total energy dissipation is lower than at low frequency or strain rates.

1.1. Challenges in Interpreting Apparent Viscosity
1.1.1. (A) Separating Spatial Variations From Frequency Dependence in Mechanical Properties
The thermodynamic state varies spatially (both laterally and radially) within the Earth setting the elastic and steady state viscosity structure. Joint inferences must consider the different spatial sampling for each process. As an example, while GIA driven by a large ice sheet such as the now-extinct Fennoscandian ice sheet is sensitive to deep ($\sim 1,000$ km) mantle structure (Lau et al., 2016), PSR processes are sensitive to much shallower (~ 100 km) Earth structure (Freed et al., 2006). Though we have attempted to minimize the geographical spread of studies in Figure 1a, the radial and lateral structure beneath the western United States may significantly contribute to discrepancies across the viscosity estimates presented. Nevertheless, these spatial variations in thermodynamic state also lead to various transient creep processes that may be activated across different regions within the planet. Transient deformation in response to forcings of different time scales may be considered as an overprint on top of elastic and steady state viscous properties.

1.1.2. (B) Reconciling Different Viscoelastic Models
Using a variety of combinations of springs and dashpots, phenomenological linear viscoelastic models can be constructed as shown in Figure S1a, described further in Text S1 (supporting information). However, the various viscosity estimates shown in Figure 1a adopt different viscoelastic models to infer Earth's "viscosity," complicating comparison of estimates from different studies. For example, the most widely used and simplest is a Maxwell model, involving a single viscosity, η_{ss}, which can be Newtonian or non-Newtonian. While this model is adopted by the majority of estimates in Figure 1b, one postseismic study used a Burgers model (Pollitz, 2003), resulting in two viscosity estimates: η_{ss} and η_t (where in Figure 1a, the lower and upper limits of the yellow box denote η_t and η_{ss}, respectively). Indeed, at other locations, similarly complicated viscoelastic models were required to fit data (e.g., for PSR see Qiu et al., 2018, or for normal modes
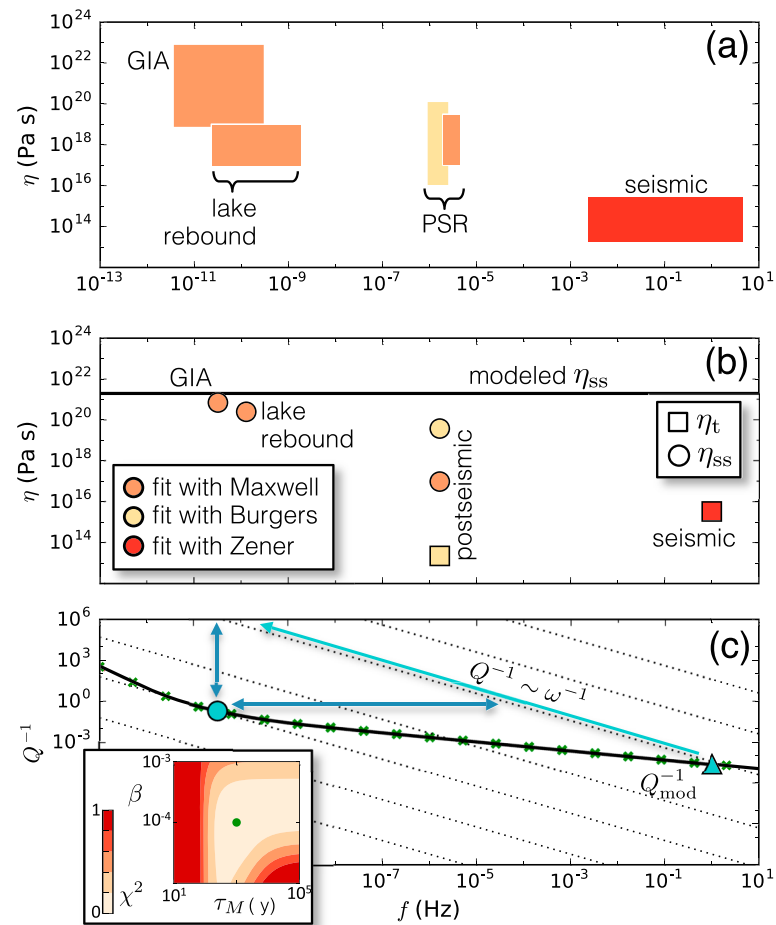
Figure 1. (a) A compilation of viscosity, η, estimates made by a variety of geophysical studies (Argus et al., 2014; Bao et al., 2016; Bills et al., 1994; Creveling et al., 2017; Dalton et al., 2008; Lau et al., 2016; Mitrovica & Forte, 2004; Pollitz et al., 2000; Pollitz, 2003). For all estimates that adopted the Maxwell model η refers to η_{ss}, while the upper and lower limits of the Burgers model postseismic estimate represent η_{ss} and η_t, respectively (Pollitz, 2003). The seismically inferred values of η represent Q^{-1} measurements converted to η_t adopting a Zener model. (b) Demonstration of estimating η_{ss} and/or η_t from synthetically produced data. The modeled value of η_{ss} is marked as a horizontal black solid line. The legend in (b) corresponds to both (a) and (b). See section 2.1 for more details. (c) The black solid line is the Q^{-1} trend of the Andrade model in panel (b). Black dotted lines mark a selection of ω^{-1} slopes. The inset shows the chi-square misfit, χ^2, as a function of the two free parameters of the Andrade model, β and τ_M (equation (S5), supporting information). See section 2.2 for more details. All panels share the same horizontal axis. GIA = glacial isostatic adjustment.

and tides see Lau & Faul, 2019). We emphasize that the choice of viscoelastic model does not provide any information on the underlying mechanistic process (e.g., the adoption of the Zener model in the seismic example does not imply anything about the possibility of diffusion or dislocation creep), which can lead to further complication in interpretation across different estimates.

1.1.3. (C) Improving Our Understanding of Deformation Mechanisms

From laboratory results and microphysical models of creep, questions remain concerning how rheological behavior measured at laboratory conditions can be extrapolated to mantle conditions and used to interpret geophysical measurements. In contrast to our relatively robust understanding of mechanisms and scaling of elasticity (e.g., Duffy & Anderson, 1989; Stixrude & Lithgow-Bertelloni, 2005) and steady state creep laws (e.g., Hansen et al., 2011; Hirth & Kohlstedt, 2003), interpretation and extrapolation of anelastic behavior has a range of unresolved problems and proposed models (Cooper, 2002; Faul & Jackson, 2015; Takei et al., 2014; Takei, 2017). General consensus, however, suggests that on top of Maxwell viscoelastic behavior, there exists a so-called "high-temperature background" (HTB) attenuation. The Extended Burgers (favored by, e.g., Jackson & Faul, 2010) and Andrade (favored by, e.g., Sundberg & Cooper, 2010) models, have been used to fit

the HTB attenuation data and are both characterized by a power law frequency dependence of $\approx \frac{1}{3}$. There is emerging agreement that the process governing HTB attenuation is anelastic diffusion-accommodated grain boundary sliding (Cooper, 2002; Faul & Jackson, 2015; Morris & Jackson, 2009; Raj, 1975; Takei, 2017) that has a temperature- and grain size-dependent scaling. However, significant disagreement on how to scale the HTB attenuation to earth conditions remains.

Other dissipative mechanisms at the grain scale—such as elastically accommodated grain boundary sliding (Jackson et al., 2014; Karato, 2012, 1986; Lee & Morris, 2010), dislocation processes (Karato & Spetzler, 1990; Farla et al., 2012), melt squirt (Hammond & Humphreys, 2000; O'Connell & Budiansky, 1977), and premelting effects (Takei, 2017; Yamauchi & Takei, 2016)—are also inferred to add dissipation peaks in some experimental studies. These processes will each scale independently, and their importance in the Earth is not yet known. Dislocation processes associated with high- and low-temperature plasticity (e.g., Hansen et al., 2019) can bring the material out of the linear anelastic regime into one with a stress amplitude dependence and may be important in some contexts (e.g., Freed et al., 2012; Qiu et al., 2018). Such nonlinearity could lead to increasing dissipation (or attenuation) with increasing frequency, that is, a positive slope of $Q^{-1}(\omega)$.

1.2. Scope of This Study

Considering Figure 1a, how can we use geophysical measurements across such a broad frequency band to learn about transient creep processes and to infer the true steady state viscosity structure? Consideration of geophysical observations in spatial and temporal isolation can only take us so far. Here, we consider Challenge B, and in the spirit of O'Connell and Budiansky (1978), we develop a simple, self-consistent framework to quantify the meaning of "apparent viscosity" across broad time scales, that involves application of a simple metric, namely the *complex viscosity*, η^*. We demonstrate its practical value for interpreting processes occurring on disparate time scales in several geophysical contexts. In the supporting information, we outline the phenomenological theory and equations upon which the paper builds and demonstrate an inference of viscosity in the time domain. following we outline the issues that arise with measures of apparent viscosity (section 2). We introduce the complex viscosity, η^*, and walk through a synthetic example of its use in regard to overcoming Challenge B (section 3).

2. The Meaning of Apparent Viscosity

The physical meaning of the viscosity "trend" in Figure 1a is not evident. In practice, there are several steps taken to reach these viscosity estimates. For example, GIA observations include time-dependent elevation data of raised beaches across both Canada and Fennoscandia (Lau et al., 2017; Peltier, 2004) from which a characteristic decay time is extracted from the resultant time series (Walcott, 1972). For PSR, GPS measurements of the crustal displacement are typically used (Bürgmann & Dresen, 2008).

How these estimates can be used to contribute to our understanding of $M(\omega)$ and $Q^{-1}(\omega)$ as measures of a single, underlying broadband constitutive rheology remains unclear. In this section, we demonstrate a framework to answer these questions in three steps: (1) We adopt a synthetic underlying broadband constitutive rheology and forward model how it would appear when sampled by different geophysical processes at intervals across the broad frequency spectrum (section 2.1); (2) we explore how its properties would be misinterpreted by constitutive models appropriate only at the frequency band of observations (section 2.2). These two steps broadly mimic the current practice across different geophysical fields. Finally, (3) we outline a simple method for inference of the underlying mechanical properties (section 2.3).

2.1. Forward Calculation of Broadband Constitutive Models

To dissect Challenge B issues, we produce a synthetic set of parallel estimates from an underlying model. While any viscoelastic model could be used for this demonstration (e.g., Extended Burgers model), we choose an Andrade model (equation (S5), supporting information) for its simplicity, with values of $\beta = 10^{-4}$, $n = \frac{1}{3}$, $\tau_M = 1,000$ years, $M_\infty = 60$ GPa, where the corresponding value of η_{ss} is shown in Figure 1b. All quantities associated with this Andrade model will be labeled with the subscript "mod" in Figure 1c.

Next, using the equations in Text S1 (supporting information), we calculate the viscosity values that would be inferred from five typical observational studies performed at four different frequency bands: GIA, lake rebound, PSR, and seismic wave propagation. The GIA, lake rebound, and PSR studies adopt a Maxwell model producing estimates of η_{ss}. (Here we have used of synthetic observations of Q^{-1} at a given frequency. For some of these processes data are available in the form of a time series and so in Text S2 (supporting

information) we walk through an example of extracting η_{ss} from a GIA-like observation and how the estimate eventually fits into this framework.) We repeat the PSR study instead using a Burgers model (thus producing estimates of η_{ss} and η_t), while for the seismic study, we will adopt a Zener model resulting in an estimate of η_t.

To produce these estimates, we sample Q^{-1}_{mod} at the respective frequencies of each study (e.g., for the GIA estimate, we will take $Q^{-1}_{mod}|_{\omega=\text{GIA band}}$). These discrete Q^{-1}_{mod} values will represent the observations for each study. For all of these studies, we make the approximation that the value for M_∞ and where appropriate M_t, is that measured the seismic band (i.e., $[M_\infty, M_t] \approx M_{mod}|_{\omega=1\text{Hz}}$), which is precisely what all the studies featured in Figure 1a assumed. (Take, e.g., GIA-based viscosity estimates made by Kaufmann & Lambeck, 2002 or Peltier, 2004, who imposed the seismic reference profile PREM; Dziewonski & Anderson, 1981 to represent M_∞.) This approximation is most likely inappropriate when considering spatial and frequency variations of $Q^{-1}(\omega)$ across the seismic band. However, when considering much longer frequency processes like GIA, such an approximation is more reasonable. Here, for the Maxwell estimates, the inferred η_{ss} values are found by applying the definition of Q^{-1} (equation (S6), supporting information) and substituting the expression for M_M (equation (S2), supporting information).

Finally, the value of ω corresponds to the frequency band of the process in question. Thus, for the Maxwell estimates, η_{ss} can be determined. For the PSR Burgers estimate, we perform a parameter search for η_{ss} and η_t. For the seismic wave propagation study, Q^{-1} estimates have been translated to the equivalent viscosity by adopting a Zener model (applying relations equations (S3) and (S6), supporting information). The resulting estimates of viscosity are shown in Figure 1b. Just as with Figure 1a, Figure 1b shows a similar trend. As can be seen, none of these studies reproduce the modeled value of η_{ss}, but within the framework of mapping out $Q^{-1}_{mod}(\omega)$ and $M_{mod}(\omega)$, η_{ss} is a necessary parameter and has physical meaning as the long-term, steady state viscosity of the Earth.

2.2. Why Do We Misestimate η_{ss}?

The mis-estimates of η_{ss} can be explained by a bias in the way that these values are derived. The same biases evident in Figure 1b using synthetic observations of Q^{-1} will still remain when using these other geophysical observations of dissipation. Let us consider the GIA example. We attempt to fit the observed Q^{-1} measurement extracted from Q^{-1}_{mod} at the GIA frequency band. While Q^{-1} is not generally used in GIA studies, we use it here as an objective measure of dissipation, equation (S6) (supporting information). This observed value of Q^{-1} is marked by the cyan circle in Figure 1c. The common approximation to use for a Maxwell model is

$$Q^{-1} \approx \frac{M_\infty}{\omega \eta_{ss}} \tag{1}$$

(derived from equations (S2) and (S6), supporting information, with the commonly adopted approximation below equation (S6), the slope for which is marked in Figure 1c with black dotted lines). We have two pieces of information at hand: M_∞ which we assume to be provided by seismic data, falling at $\omega = 1$ Hz (the cyan triangle in Figure 1c) and the observed Q^{-1} marked by the left circle at the GIA band. Thus, we are left with inconsistent values that cannot fall on any single dotted line where

$$\eta_{ss} \approx \frac{M|_{\omega=1\text{ Hz}}}{\omega_{GIA} \times Q^{-1}|_{\omega=GIA}}. \tag{2}$$

The result is that either the frequency we are imposing or the observed Q^{-1} values are too low for the corresponding M value. That is, a simple Maxwell model cannot capture the departure from linearity exhibited by Q^{-1}_{mod}. This thought process may be extended to the misfit evident in the other estimates of η_{ss}.

We note that the closest estimate to modeled η_{ss} is the GIA-based estimate, whereas toward higher frequencies, the departure of the estimates increases. This result is intuitive, as the GIA band is the lowest frequency process and thus deformation is viscously dominated. It is possible that η_{ss}, as estimated by GIA, might indeed be close to the modeled η_{ss}, supported by the fact that viscosity estimates from both GIA and mantle convection studies (acting on even longer time scales) can be consistent Mitrovica and Forte (2004). In this example, it reflects our chosen value of $\tau_M = 1,000$ years. Nevertheless, more work needs to be done to verify this and the systematic bias, present in all our estimates shown in Figure 1b, remains cause for concern.

2.3. A Simple Inference of the Underlying Model

As a simple demonstration, we show, through a parameter search, that with two measurements of Q^{-1} at the GIA and PSR time scales, Q_{mod}^{-1} can be recovered accurately in this hypothetical example. The inset in Figure 1c shows the chi-square misfit, χ^2, as a function of the two free parameters of the Andrade model, β and τ_{M}. The green-solid circle marks β_{mod} and τ_{mod} used to produce Q_{mod}^{-1}. The minimum value of χ^2 coincides with these modeled values and the green × symbols in Figure 1c is the resulting Q^{-1} trend calculated using these fitted values. From the estimate of τ_{mod}, η_{ss} can be extracted assuming the seismically inferred M_∞.

We acknowledge that this is an extremely simplistic demonstration of a framework for finding the modeled value of η_{ss}, but this exercise is not the focus of this paper. While it is clear the Maxwell model should not be expected to reproduce the behavior of the Andrade model, the main message here is that, if transient creep is occuring (here represented by the Andrade model), using a Maxwell model would recover an erroneous estimate of η_{ss}, even though this is common practice (see also Text S2, supporting information). Only if transient creep is incorporated as a possibility can one assess whether $\eta = \eta_{\mathrm{ss}}$. We note that other phenomenological models may be more suitable than the two-parameter Andrade model used here and emphasize that our choice of the model is for demonstrative purposes.

3. Complex Viscosity η^*

In an attempt to further develop a unifying view of dissipation across the broad spectrum of geophysical processes, we propose the use of the "complex viscosity," a parameter (and concept) to assist in the comparison of viscosity estimates from across the spectrum. We derive it here and then apply it in section 3.2 to the case introduced in section 2.1.

3.1. Theory

The complex viscosity, η^*, appears (obscurely) in the continuum mechanics literature (Christensen, 1971; Cox & Merz, 1958) and came to our attention in reading about the rheology of cheese Gunasekaran and Ak (2002). η^* is complementary to the (complex) modulus M (e.g., equations (S2)–(S5), supporting information), derived as follows. If we apply an oscillatory stress, $\sigma_0 e^{i\omega t}$, to a viscoelastic medium of modulus, $M(\omega)$, it is related to the strain, ε, with the following form:

$$\sigma_0 e^{i\omega t} = M(\omega)\varepsilon_0 e^{i\omega t}. \tag{3}$$

Upon taking the strain rate, the complex viscosity is

$$\sigma_0 e^{i\omega t} = \eta^*(\omega)\left[\frac{\mathrm{d}}{\mathrm{d}t}\varepsilon_0 e^{i\omega t}\right] = \eta^*(\omega)\left[i\omega\varepsilon_0 e^{i\omega t}\right]. \tag{4}$$

Thus, it can be seen that η^* is simply

$$\eta^*(\omega) = -\frac{i}{\omega}M(\omega). \tag{5}$$

It is important to highlight that, unlike the viscosities we have previously discussed, η^* is a function of frequency just as $M(\omega)$ is, and, like $M(\omega)$, η_X^* may be derived for a given viscoelastic model X using the relation give by equation (5). Intuitively, it is a normalized version of $M(\omega)$; however, η_1^* is the attenuative component and η_2^* is the dispersive component (where $\eta^* = \eta_1^* + i\eta_2^*$). The minus sign flips the quantity so that it represents the proportion of viscous dissipation. We define the magnitude of η^* as

$$\|\eta^*\| = \left[(\eta_1^*)^2 + (\eta_2^*)^2\right]^{1/2}, \tag{6}$$

where $\|\eta^*\|$ of several viscoelastic models is shown in Figure 2a, for which we have chosen identical values of η_{ss} and M_∞ which results in similar high and low frequency behavior. The values for all parameters are listed in the figure caption.

As can be seen, $\|\eta^*\|$ decreases with increasing frequency for all models. At low frequency, $\|\eta^*\|$ values all converge to η_{ss}, with the exception of the Zener model which, due to the lack of a steady state viscous dashpot, $\|\eta_Z^*\| \to \infty$ as $\omega \to 0$ along a slope of ω^{-1}. At this limit, $\|\eta^*\|$ represents the maximum portion of viscous dissipation. Increasing frequency from the steady state, toward and beyond $1/\tau_{\mathrm{M}}$ (black-dashed vertical line), $\|\eta^*\|$ becomes frequency dependent where viscous dissipation diminishes. The inset of Figure 2a
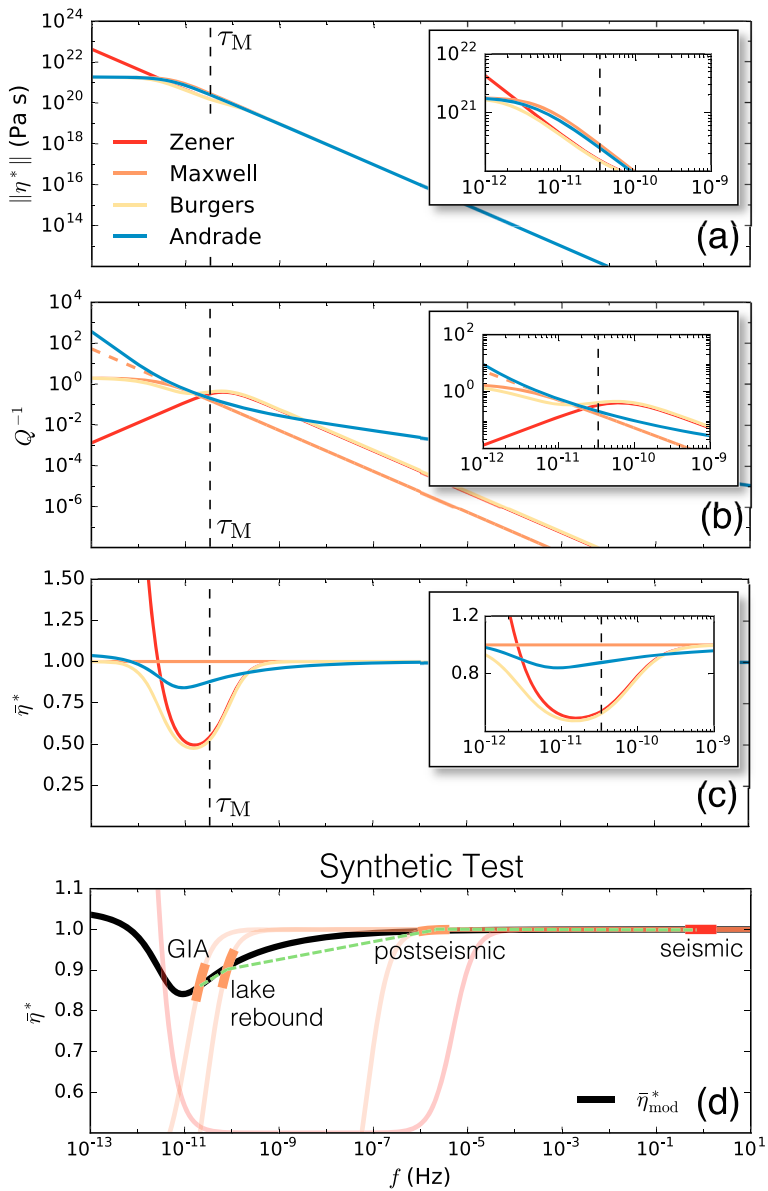
Figure 2. Measures of dissipation for viscoelastic models (Figure S1a, supporting information): (a) the magnitude of complex viscosity, $\|\eta^*\|$ (equation (6)); (b) the attenuation, Q^{-1} (equation (S6), supporting information); and (c) the normalized complex viscosity, $\bar{\eta}^*$ (equation (8)). The legend in panel (a) corresponds to panels (a)–(c), the vertical black dashed line marks the Maxwell time, τ_M (equation (S1), supporting information), and these panels are accompanied by insets that focus on the main panel within the vicinity of the Maxwell time, τ_M. For all viscoelastic models, where relevant, $\eta_{ss} = 2 \times 10^{21}$ Pa s, $\eta_t = \eta_{ss}/10$, $M_\infty = 60$ GPa, and $M_t = 0.8 \times M_\infty$ (see equations (S2)–(S4), supporting information). In addition, for the Andrade model, $\beta = 10^{-4}$ (equation (S5), supporting information). Panel (b) includes the full expression of Q^{-1} for the Maxwell model (equation (S6), supporting information; solid orange line) and the approximate version (where $Q^{-1} \approx M_2/M_1$, dashed orange line). (d) Synthetic example of fitting the modeled $\bar{\eta}^*$ trend (equation (8); black solid line) with discrete observations that adopted Maxwell models (orange lines; GIA, lake rebound and postseismic data) and a Zener model (red line; seismic). These fits correspond to the synthetic estimates of η_{ss} and η_t shown in Figure 1b. See section 3 for more details. All panels share the same horizontal axis. GIA = glacial isostatic adjustment.

focuses on $\|\eta^*\|$ around the vicinity of τ_M, and here the $\|\eta^*\|$ values across the viscoelastic models depart from each other. This highlights the differing transient nature of all models with exception to the Maxwell model (which does not exhibit transient behavior).

Figure 2b shows the corresponding Q^{-1} trends for our viscoelastic models. We note that the approximation of Q^{-1} for the Maxwell model (i.e., $Q^{-1} \approx M_2/M_1$; dashed orange line) and the full expression (equation (S6), supporting information; solid orange line) diverge at low frequency. As can been seen, departures across the viscoelastic models exist across the entire frequency band. In contrast, the most prominent differences in $\|\eta^*\|$ across all models is isolated across the transient regime—the precise behavior we are interested in.

To further isolate and highlight transient behavior, we will normalize $\|\eta^*\|$ by $\|\eta_M^*\|$, which we will refer to as the reference (Maxwell) model (with the same η_{ss} and M_∞ values), where

$$\eta_M^* = -\frac{i}{\omega}\left[\frac{i\omega\eta_{ss}}{1 + i\omega\frac{\eta_{ss}}{M_\infty}}\right] = \frac{\eta_{ss}}{1 + i\omega\frac{\eta_{ss}}{M_\infty}}, \tag{7}$$

and for a given viscoelastic model X, this normalized quantity, $\bar{\eta}^*_X$, is

$$\bar{\eta}_X^*(\omega) \equiv \frac{\|\eta_X^*(\omega)\|}{\|\eta_M^*(\omega)\|}. \tag{8}$$

Figure 2c shows this quantity for all the viscoelastic models. If $\bar{\eta}^*$ is unity, at that given frequency the viscoelastic model is behaving very similarly to the Maxwell model. With exception to the Zener model, all models lie at unity at both low and high-frequency limits. In between the two limits, centered around τ_M, we see the transient behaviors of each model, which in all cases lie beneath the reference Maxwell model due to the presence of increased dissipation across the transient band. It is this dissipation highlighted by the new $\bar{\eta}^*$ quantity that holds valuable information on the frequency-dependent nature of transient creep.

We note two issues in regard to $\bar{\eta}^*$ in Figure 2c: (1) At the low frequency extreme, $\bar{\eta}_A^*$ exceeds 1 due to the additional contribution of dissipation from the transient component of the Andrade model (see Text S1, supporting information). (2) The divergence in Q^{-1} between Maxwell and the anelastic models (Burgers and Andrade) at the high-frequency extreme (see Figure 2b) implies increased dissipation relative to Maxwell, but $\bar{\eta}^*$ (Figure 2c) shows convergence to 1 at this frequency range. The two measures give complementary information: $\bar{\eta}^*$ is making a broader point that the deformation is by far predominantly elastic; the ratio Q^{-1} demonstrates more subtle differences.

3.2. Extending the Framework for Inference of η

Having introduced $\bar{\eta}^*$, we extend the synthetic fitting exercise of section 2. Once more, we were left with conflicting estimates of η_{ss} and η_t from a variety of processes and viscoelastic models, none of which reproduced the modeled η_{ss} value (Figure 1b). However, there is useful information within these discrete inferences and here we propose a framework to collectively interpret these estimates based around $\bar{\eta}^*$.

We wish to recover our forward model $\bar{\eta}_{mod}^*$ (black solid line in Figure 2d, corresponding to Q_{mod}^{-1} in Figure 1c). Our first task is to determine the most accurate value of $\|\eta_M^*\|$ for normalization. This requires an estimate of η_{ss} and M_∞. As with our previous example, M_∞ will come from seismic estimates (i.e., $M_\infty \approx M|_{\omega=1\,Hz}$), but one must take care with η_{ss} and not make the mistake of assuming the linearity of the Maxwell model (section 2). As such, we will use the value of τ_M determined by the simple parameter search exercise we performed in section 2.3 (see inset of Figure 1c) to produce η_M^*.

With the observations available to us, we will determine their corresponding $\bar{\eta}^*_X$ for each viscoelastic model X, using the η_{ss} and η_t values inferred (Figure 1b). These are shown in Figure 2d as faded lines (orange for Maxwell fits and red for the Zener model fit). It is clear that $\bar{\eta}_X^*$ trends do not fit $\bar{\eta}_{mod}^*$ across all frequencies. This is expected, as they were only made to fit the black solid line across their respective frequency bands. As such, each study is valid only across its associated frequency band and the partial solid colored lines coincident with the solid faded lines highlight this region of validity for each estimate. As an example, consider the orange line in Figure 2d labeled "GIA." The faded solid orange line that spans the whole frequency range of the figure is $\bar{\eta}^*_M$ (i.e., a Maxwell model) where the parameters used were found by fitting the GIA observation. The partial solid orange line marks the frequency range across which those parameters were fit.

By considering these disparate estimates of $\|\bar{\eta}^*\|$ only across their frequency band of validity, it is then possible to map out an approximate frequency dependence from the unrelaxed to steady state limit. In this hypothetical exercise, one possible trend drawn from the available data could be the green-dashed line. Thus this simple exercise demonstrates that from four distinct viscosity studies which adopted a range of different viscoelastic models, it is possible to estimate the transient behavior in a coherent and consistent manner. Eventually, it should be possible to interpolate between these observations using microphysics and laboratory-derived constitutive models.

4. Concluding Remarks

To build a coherent picture of Earth's deformation across the broad frequency band, many geophysical studies that employ a variety of viscoelastic models at different time scales and geological environments must be consistently combined. However, the field must overcome the three challenges defined in section 1.1. In regard to Challenge A, we must develop methologies that can simultaneously incorporate spatial variations and frequency dependence in mechanical properties. Regarding Challenge C, our evolving understanding of transient deformation mechanisms must be appropriately incorporated into larger-scale geophysical problems.

Here we have focused on Challenge B and suggest the use of a new parameter, the complex viscosity, which when applied correctly can bring together conclusions from a variety of geophysical studies that adopt different viscoelastic models (e.g., Maxwell, Burgers models). If combined with experimental inferences on the frequency dependence of viscoelastic dissipation, we believe that the complex viscosity may prove to be a simple yet illuminating parameter for the coherent analysis of dynamics across geophysical time scales.

References

Argus, D. F., Peltier, W. R, Drummond, R., & Moore, A. W. (2014). The Antarctica component of postglacial rebound model ICE-6G_C (VM5a) based on GPS positioning, exposure age dating of ice thicknesses, and relative sea level histories. *Geophysical Journal International*, *198*, 537–563. https://doi.org/10.1093/gji/ggu140

Bao, X., Dalton, C. A., Jin, G., Gaherty, J. B., & Shen, Y. (2016). Imaging Rayleigh wave attenuation with USArray. *Geophysical Journal International*, *206*, 241–259. https://doi.org/10.1093/gji/ggw151

Bills, B. G., Adams, K. D., & Wesnousky, S. G. (2007). Viscosity structure of the crust and upper mantle in western Nevada from isostatic rebound patterns of the late Pleistocene Lake Lahontan high shoreline. *Journal of Geophysical Research*, *112*, B06405. https://doi.org/10.1029/2005JB003941

Bills, B. G., Currey, D. R., & Marshall, G. A. (1994). Viscosity estimates for the crust and upper mantle from patterns of lacustrine shoreline deformation in the Eastern Great Basin. *Journal of Geophysical Research*, *99*, 22. https://doi.org/10.1029/94JB01192

Bürgmann, R., & Dresen, G. (2008). Rheology of the lower crust and upper mantle: Evidence from rock mechanics, geodesy, and field observations. *Annual Review of Earth and Planetary Sciences*, *36*, 531–567. https://doi.org/10.1146/annurev.earth.36.031207.124326

Christensen, R. (1971). *Theory of viscoelasticity: An introduction*. New York, NY: Academic Press.

Cooper, R. F. (2002). Seismic wave attenuation: Energy dissipation in viscoelastic crystalline solids. *Reviews in Mineralogy and Geochemistry*, *51*, 253–290. https://doi.org/10.2138/gsrmg.51.1.253

Cox, W. P., & Merz, E. H. (1958). Correlation of dynamic and steady flow viscosities. *Journal of Polymer Science*, *28*, 619–622. https://doi.org/10.1002/pol.1958.1202811812

Creveling, J. R., Mitrovica, J. X., Clark, P. U., Waelbroeck, C., & Pico, T. (2017). Predicted bounds on peak global mean sea level during marine isotope stages 5a and 5c. *Quaternary Science Reviews*, *163*, 193–208. https://doi.org/10.1016/j.quascirev.2017.03.003

Dalton, C. A., EkströM, G., & DziewońSki, A. M. (2008). The global attenuation structure of the upper mantle. *Journal of Geophysical Research*, *113*, B09303. https://doi.org/10.1029/2007JB005429

Dickinson-Lovell, H., Huang, M.-H., Freed, A. M., Fielding, E., Bürgmann, R., & Andronicos, C. (2018). Inferred rheological structure and mantle conditions from postseismic deformation following the 2010 M_w 7.2 El Mayor-Cucapah Earthquake. *Geophysical Journal International*, *213*, 1720–1730. https://doi.org/10.1093/gji/ggx546

Duffy, T. S., & Anderson, D. L. (1989). Seismic velocities in mantle minerals and the mineralogy of the upper mantle. *Journal of Geophysical Research*, *94*, 1895–1912. https://doi.org/10.1029/JB094iB02p01895

Dziewonski, A. M., & Anderson, D. L. (1981). Preliminary reference Earth model. *Physics of the Earth and Planetary Interiors*, *25*(4), 297–356. https://doi.org/10.1016/0031-9201(81)90046-7

Farla, R. J. M., Jackson, I., Fitz Gerald, J. D., Faul, U. H., & Zimmerman, M. E. (2012). Dislocation damping and anisotropic seismic wave attenuation in Earth's upper mantle. *Science*, *336*, 332. https://doi.org/10.1126/science.1218318

Faul, U., & Jackson, I. (2015). Transient creep and strain energy dissipation: An experimental perspective. *Annual Review of Earth and Planetary Sciences*, *43*(1), 541–569. https://doi.org/10.1146/annurev-earth-060313-054732

Freed, A. M., Burgmann¨, R., Calais, E., Freymueller, J., & Hreinsdottir, S. (2006). Implications of deformation following the 2002 Denali, Alaska, earthquake for postseismic relaxation processes and lithospheric rheology. *Journal of Geophysical Research*, *111*, B01401. https://doi.org/10.1029/2005JB003894

Freed, A. M., Hirth, G., & Behn, M. D. (2012). Using short-term postseismic displacements to infer the ambient deformation conditions of the upper mantle. *Journal of Geophysical Research*, *117*, B01409. https://doi.org/10.1029/2011JB008562

Gunasekaran, S., & Ak, M. (2002). *Cheese rheology and texture*. Boca Raton, FL: CRC Press.

Hammond, W. C., & Humphreys, E. D. (2000). Upper mantle seismic wave velocity: Effects of realistic partial melt geometries. *Journal of Geophysical Research*, *105*, 10. https://doi.org/10.1029/2000JB900041

Hansen, L., Kumamoto, K. M., Thom, C. A., Wallis, D., Durham, W. B., Goldsby, D. L., et al. (2019). Low-temperature plasticity in olivine: Grain size, strain hardening, and the strength of the lithosphere. *Journal of Geophysical Research: Solid Earth*, *124*, 5427–5449. https://doi.org/10.1029/2018JB016736

Hansen, L., Zimmerman, M. E., & Kohlstedt, D. L. (2011). Grain boundary sliding in San Carlos olivine: Flow law parameters and crystallographic-preferred orientation. *Journal of Geophysical Research*, *116*, B08201. https://doi.org/10.1029/2011jb008220

Hirth, G., & Kohlstedt, D. (2003). Rheology of the upper mantle and the mantle wedge: A view from the experimentalists. *Washington DC American Geophysical Union Geophysical Monograph Series*, *138*, 83–105. https://doi.org/10.1029/138GM06

Jackson, I., & Faul, U. H. (2010). Grainsize-sensitive viscoelastic relaxation in olivine: Towards a robust laboratory-based model for seismological application. *Physics of the Earth and Planetary Interiors*, *183*(1-2), 151–163. https://doi.org/10.1016/j.pepi.2010.09.005

Jackson, I., Faul, U. H., & Skelton, R. (2014). Elastically accommodated grain-boundary sliding: New insights from experiment and modeling. *Physics of the Earth and Planetary Interiors*, *228*, 203–210. https://doi.org/10.1016/j.pepi.2013.11.014

Karato, S. (1986). Does partial melting reduce the creep strength of the upper mantle? *Nature*, *319*, 309–310. https://doi.org/10.1038/319309a0

Karato, S.-i. (2012). On the origin of the asthenosphere. *Earth and Planetary Science Letters*, *321*, 95–103. https://doi.org/10.1016/j.epsl.2012.01.001

Karato, S., & Spetzler, H. A. (1990). Defect microdynamics in minerals and solid state mechanisms of seismic wave attenuation and velocity dispersion in the mantle. *Reviews of Geophysics*, *28*, 399–421. https://doi.org/10.1029/RG028i004p00399

Kaufmann, G., & Lambeck, K. (2002). Glacial isostatic adjustment and the radial viscosity profile from inverse modeling. *Journal of Geophysical Research*, *107*, 2280. https://doi.org/10.1029/2001JB000941

Lau, H. C., & Faul, U. H. (2019). Anelasticity from seismic to tidal timescales: Theory and observations. *Earth and Planetary Science Letters*, *508*, 18–29. https://doi.org/https://doi.org/10.1016/j.epsl.2018.12.009

Lau, H. C. P., Faul, U., Mitrovica, J. X., Al-Attar, D., Tromp, J., & Garapić, G. (2017). Anelasticity across seismic to tidal timescales: A self-consistent approach. *Geophysical Journal International*, *208*, 368–384. https://doi.org/10.1093/gji/ggw401

Lau, H. C. P., Mitrovica, J. X., Austermann, J., Crawford, O., Al-Attar, D., & Latychev, K. (2016). Inferences of mantle viscosity based on ice age data sets: Radial structure. *Journal of Geophysical Research: Solid Earth*, *121*, 6991–7012. https://doi.org/10.1002/2016JB013043

Lee, L. C., & Morris, S. J. S. (2010). Anelasticity and grain boundary sliding. *Proceedings of the Royal Society of London Series A*, *466*, 2651–2671. https://doi.org/10.1098/rspa.2009.0624

Lekic, V., French, S. W., & Fischer, K. M. (2011). Lithospheric thinning beneath rifted regions of Southern California. *Science*, *334*(6057), 783–787. https://doi.org/10.1126/science.1208898

Mitrovica, J. X., & Forte, A. M. (2004). A new inference of mantle viscosity based upon joint inversion of convection and glacial isostatic adjustment data. *Earth and Planetary Science Letters*, *225*, 177–189. https://doi.org/10.1016/j.epsl.2004.06.005

Morris, S., & Jackson, I. (2009). Diffusionally assisted grain-boundary sliding and viscoelasticity of polycrystals. *Journal of the Mechanics and Physics of Solids*, *57*(4), 744–761. https://doi.org/10.1016/j.jmps.2008.12.006

Nimmo, F., & Faul, U. H. (2013). Dissipation at tidal and seismic frequencies in a melt-free, anhydrous Mars. *Journal of Geophysical Research: Planets*, *118*, 2558–2569. https://doi.org/10.1002/2013JE004499

Nishimura, T., & Thatcher, W. (2003). Rheology of the lithosphere inferred from postseismic uplift following the 1959 Hebgen Lake earthquake. *Journal of Geophysical Research*, *108*(B8), 2389. https://doi.org/10.1029/2002JB002191

O'Connell, R. J., & Budiansky, B. (1977). Viscoelastic properties of fluid-saturated cracked solids. *Journal of Geophysical Research*, *82*, 5719–5735. https://doi.org/10.1029/JB082i036p05719

O'Connell, R. J., & Budiansky, B. (1978). Measures of dissipation in viscoelastic media. *Geophysical Research Letters*, *5*, 5–8. https://doi.org/10.1029/GL005i001p00005

Peltier, W. R. (2004). Global glacial isostasy and the surface of the ice-age Earth: The ICE-5G (VM2) Model and GRACE. *Annual Review of Earth and Planetary Sciences*, *32*, 111–149. https://doi.org/10.1146/annurev.earth.32.082503.144359

Pollitz, F. F. (2003). Transient rheology of the uppermost mantle beneath the Mojave Desert, California. *Earth and Planetary Science Letters*, *215*, 89–104. https://doi.org/10.1016/S0012-821X(03)00432-1

Pollitz, F. F., Peltzer, G., & Bürgmann, R. (2000). Mobility of continental mantle: Evidence from postseismic geodetic observations following the 1992 Landers earthquake. *Journal of Geophysical Research*, *105*, 8035–8054. https://doi.org/10.1029/1999JB900380

Qiu, Q., Moore, J. D. P., Barbot, S., Feng, L., & Hill, E. M. (2018). Transient rheology of the Sumatran mantle wedge revealed by a decade of great earthquakes. *Nature Communications*, *9*, 995. https://doi.org/10.1038/s41467-018-03298-6

Raj, R. (1975). Transient behavior of diffusion-induced creep and creep rupture. *Metallurgical Transactions A*, *6*(8), 1499–1509. https://doi.org/10.1007/BF02641961

Stixrude, L., & Lithgow-Bertelloni, C. (2005). Thermodynamics of mantle minerals—I. Physical properties. *Geophysical Journal International*, *162*, 610–632. https://doi.org/10.1111/j.1365-246X.2005.02642.x

Sundberg, M., & Cooper, R. F. (2010). A composite viscoelastic model for incorporating grain boundary sliding and transient diffusion creep; correlating creep and attenuation responses for materials with a fine grain size. *Philosophical Magazine*, *90*, 2817–2840. https://doi.org/10.1080/14786431003746656

Takei, Y. (2017). Effects of partial melting on seismic velocity and attenuation: A new insight from experiments. *Annual Review of Earth and Planetary Sciences*, *45*, 447–470. https://doi.org/10.1146/annurev-earth-063016-015820

Takei, Y., Karasawa, F., & Yamauchi, H. (2014). Temperature, grain size, and chemical controls on polycrystal anelasticity over a broad frequency range extending into the seismic range. *Journal of Geophysical Research: Solid Earth*, *119*, 5414–5443. https://doi.org/10.1002/2014JB011146

Walcott, R. (1972). Late Quaternary vertical movements in eastern North America: Quantitative evidence of glacio-isostatic rebound. *Reviews of Geophysics*, *10*, 849–884.

Yamauchi, H., & Takei, Y. (2016). Polycrystal anelasticity at near-solidus temperatures. *Journal of Geophysical Research: Solid Earth*, *121*, 7790–7820. https://doi.org/10.1002/2016JB013316